Supporting Information

Stabilizing Lithium Metal Anodes via Tuned Li^+–π Interactions in Nanoporous Porous Aromatic Framework-Coated Separators

Beom Gwon Son,[a] Hye Ryung Byon,[b] Sangtae Kim,*[c] and Eun Seon Cho*[a]

[a] *Department of Chemical and Biomolecular Engineering, Korea Advanced Institute of Science and Technology (KAIST), Daejeon, 34141, Republic of Korea*

[b] *Department of Chemistry, Korea Advanced Institute of Science and Technology (KAIST), Daejeon 34141, Republic of Korea*

[c] *Department of Materials Science and Engineering, Hanyang University, Seoul 04763, Republic of Korea*

*corresponding author: escho@kaist.ac.kr; sangtae@hanyang.ac.kr

Characterization and Instrumentation

Fourier transform infrared spectroscopy (FT-IR) measurements were carried out over a range of 4000-400 cm^{-1} (Bruker ALPHA-P). The content of C, H and N in PAF was determined by elemental analysis (EA, Thermo Scientific Flash 2000 analyzer, KAIST Analysis Center for Research Advancement (KARA)). The chemical functional groups of graphene layers were analyzed using X-ray photoelectron spectroscopy with monochromatic Al Kα as an excitation source (XPS, KALPA, Thermo VG Scientific, KARA), and spectra were calibrated to the C 1*s* peak at 284.6 eV. The specific surface areas and pore size distributions of PAF samples were obtained from N_2 isotherms using the Brunauer-Emmet-Teller (BET) and Barrett-Joyner-Halenda (BJH) methods (Tristar II 3020, Micromeritics) after degassing at 120 °C. ^{1}H and ^{7}Li NMR spectra were acquired with a Bruker AVIII 400. Morphologies of PAF-coated separators were observed by field emission scanning electron microscopy (FE-SEM, SU5000, Hitachi, KARA). Raman spectra were acquired using a dispersive Raman spectrometer with a 532 nm excitation source (ARAMIS, Horiba Jobin Yvan, KARA).

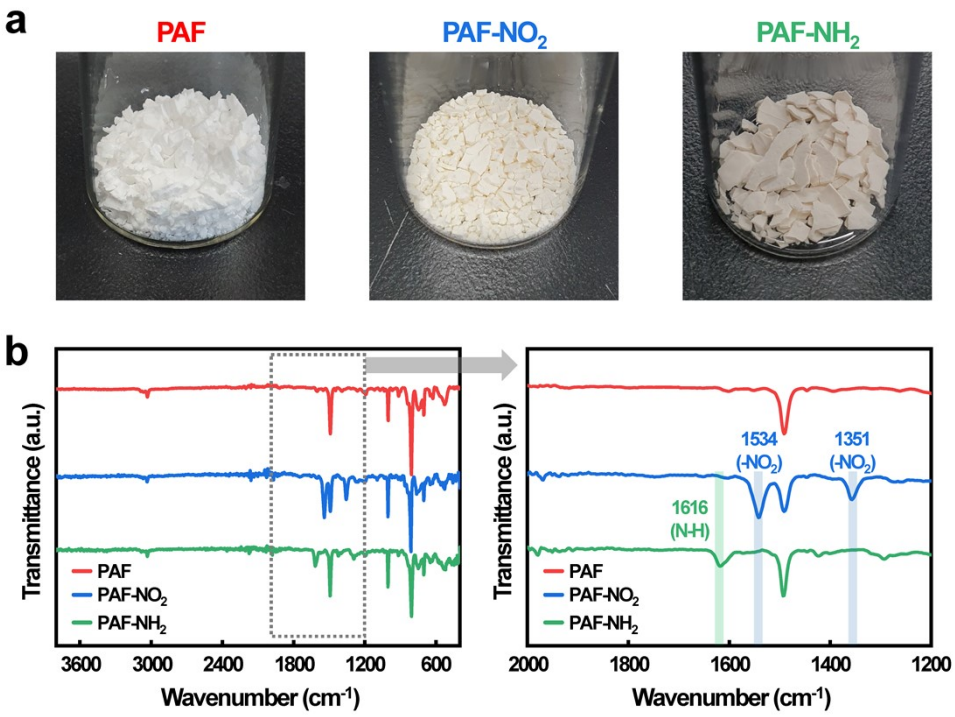

Fig. S1 (a) Color change upon the introduction of nitro (PAF-NO_2) and amino (PAF-NH_2) groups into the PAF structure. (b) FT-IR spectra of pristine PAF and N-functionalized PAFs.

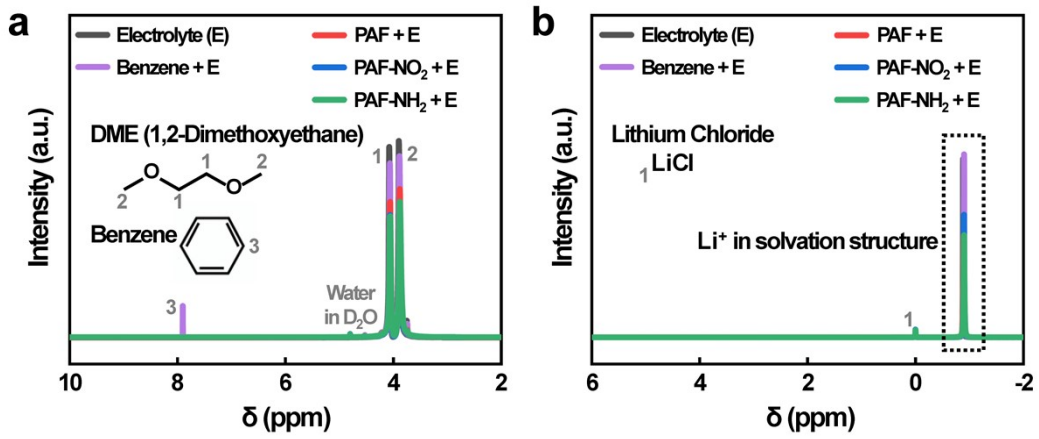

Fig. S2 Characteristics of benzene- and PAFs-dispersed electrolyte solutions: (a) ^{1}H and (b) ^{7}Li NMR spectra (10 mg/mL in 1 M LiFSI/DME with 0.3 M $LiNO_3$). For NMR measurements, the NMR tube was filled with the electrolyte in which benzene or PAFs were dispersed, while a capillary tube sealed with a polytetrafluoroethylene (PTFE) cap and filled with 1 M LiCl dissolved in D_2O was inserted into the NMR tube and used as an external reference. The chemical shifts were referenced to the water signal in D_2O at 4.8 ppm for ^{1}H NMR and to the Li^+ signal in LiCl at 0 ppm for ^{7}Li NMR, using the external reference.

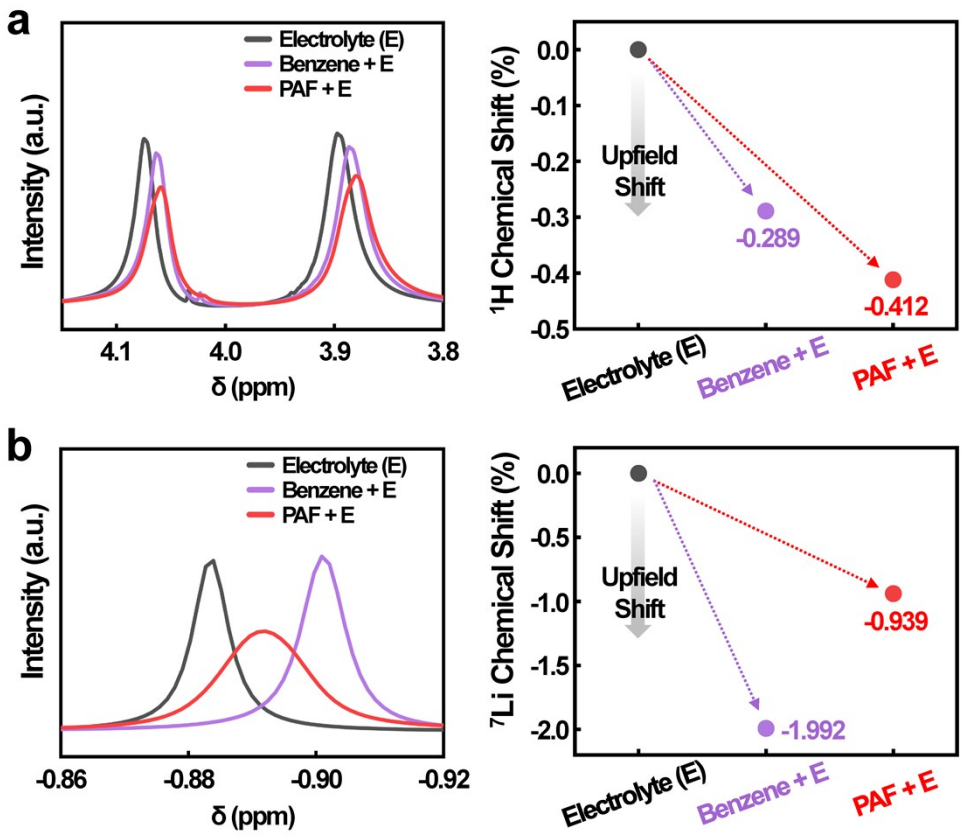

Fig. S3 Characteristics of benzene- and PAF-dispersed electrolyte solutions: (a) ^{1}H and (b) ^{7}Li NMR spectra (prepared at a concentration of 10 mg/mL) with the relative changes in peak positions.

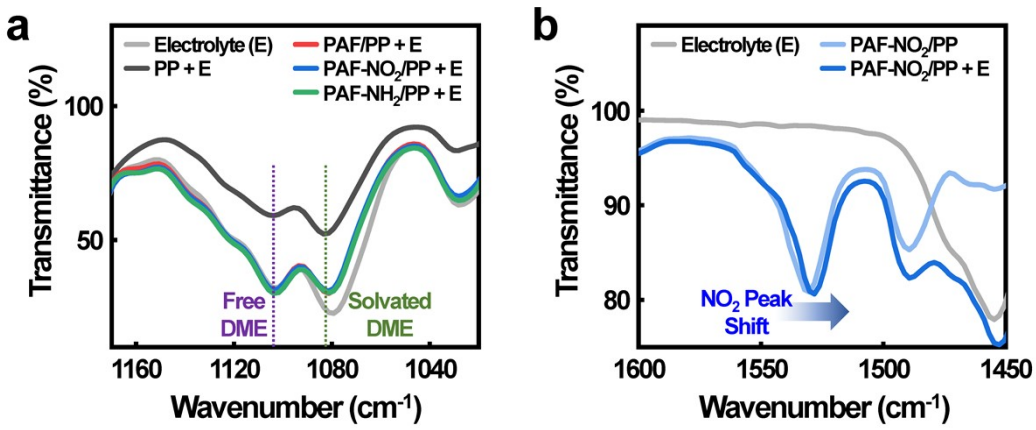

Fig. S4 (a) FT-IR spectra of PAF- and N-functionalized PAF-coated PP separators after electrolyte impregnation. (b) FT-IR spectra of PAF-NO_2/PP separator before and after electrolyte impregnation, showing the shift of the NO_2 peak.

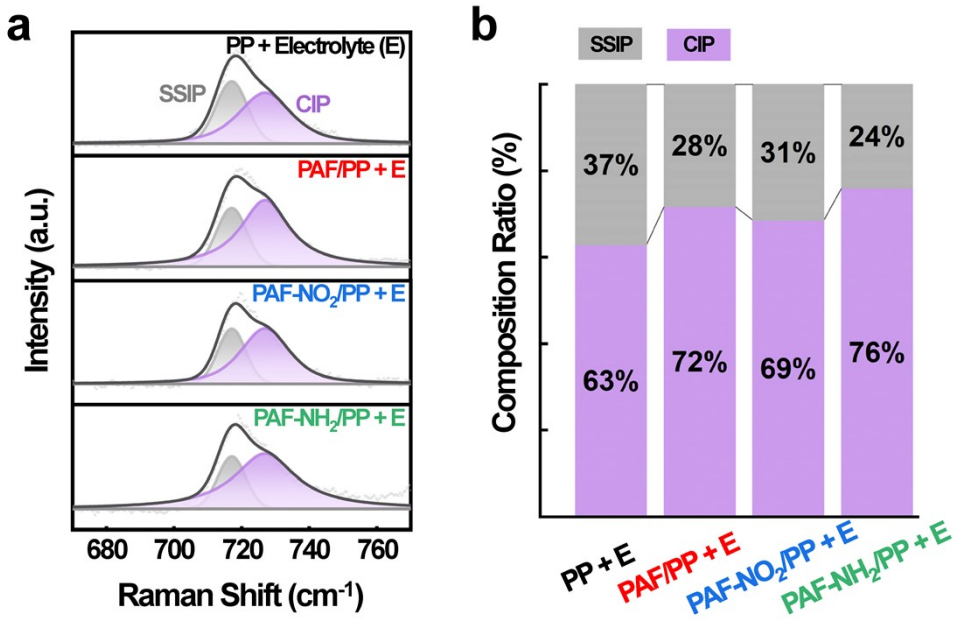

Fig. S5 (a) Raman spectra of PAF- and N-functionalized PAF-coated PP separators after electrolyte impregnation, highlighting Li^+ solvation structures represented by solvent-separated ion pairs (SSIPs) to contact ion pairs (CIPs). (b) Ratio of SSIP to CIP in Li^+ solvation structures.

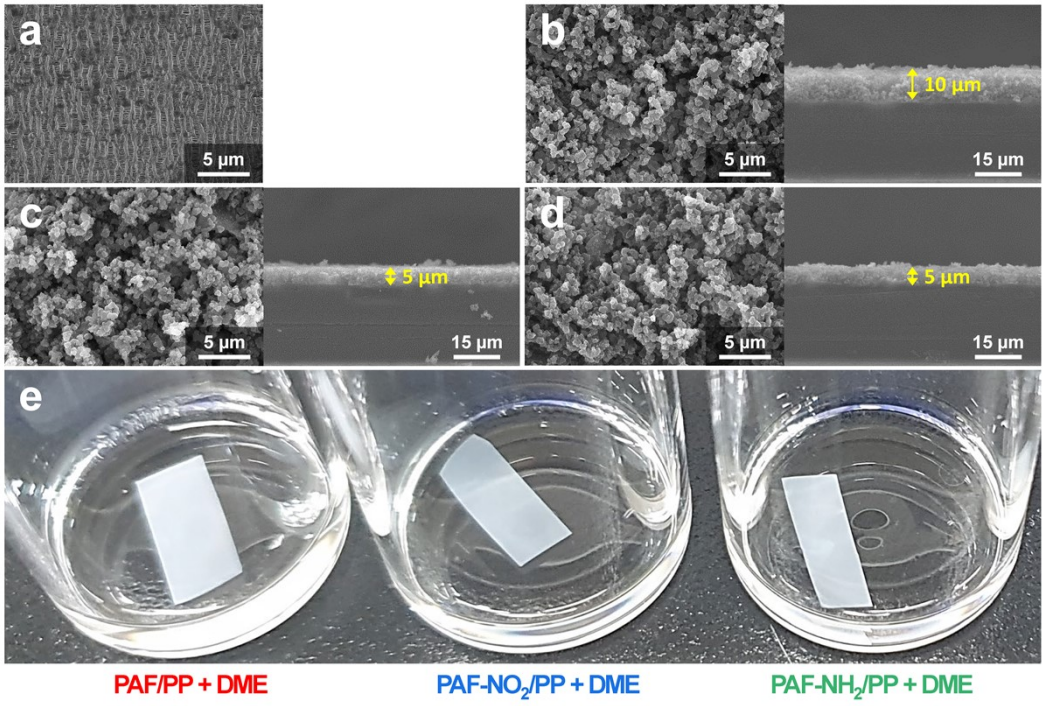

Fig. S6 FE-SEM images of (a) bare PP (Celgard 2500), (b) PAF-, (c) PAF-NO_2-, and (d) PAF-NH_2-coated separators on the coated-surface and cross-sectional views (mass loading = 0.10 mg/cm^2). (e) Photos of PAF-coated separators immersed in DME electrolyte solvent, demonstrating the enhanced stability afforded by the incorporation of a binder (CMC/SBR 1:1 wt %).

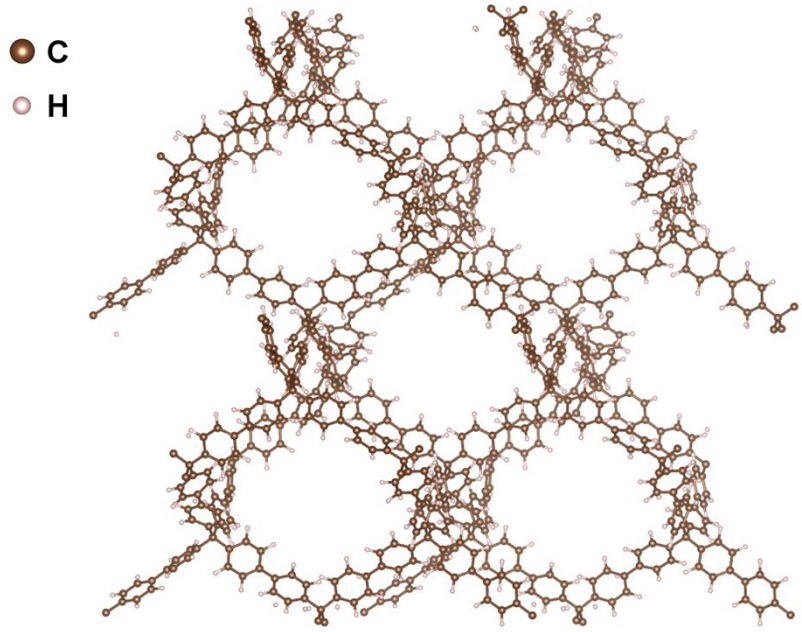

Fig. S7 The modeled crystalline PAF structure with repeating unit cells.

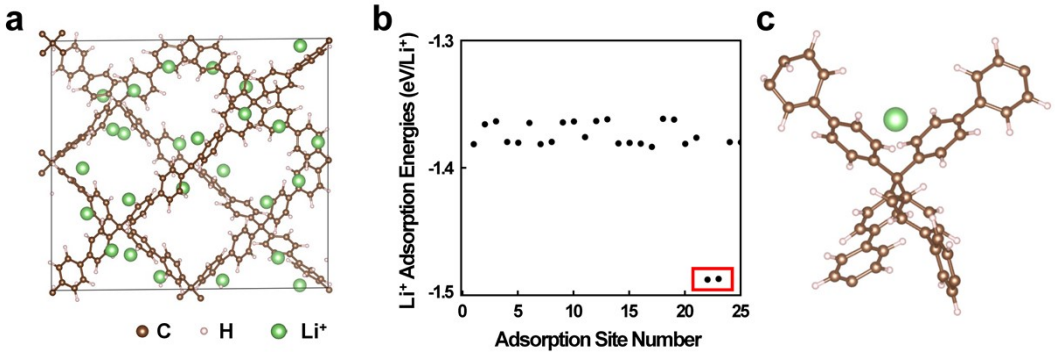

Fig. S8 (a) Schematic illustration of the 25 Li^+ adsorption sites considered in the model. (b) The computed Li^+ adsorption energies for each site and (c) the optimized atomic configurations of the two sites with strengthened Li^+ adsorption (highlighted with red boxes in (b)), where Li^+ is positioned between two phenyl rings.

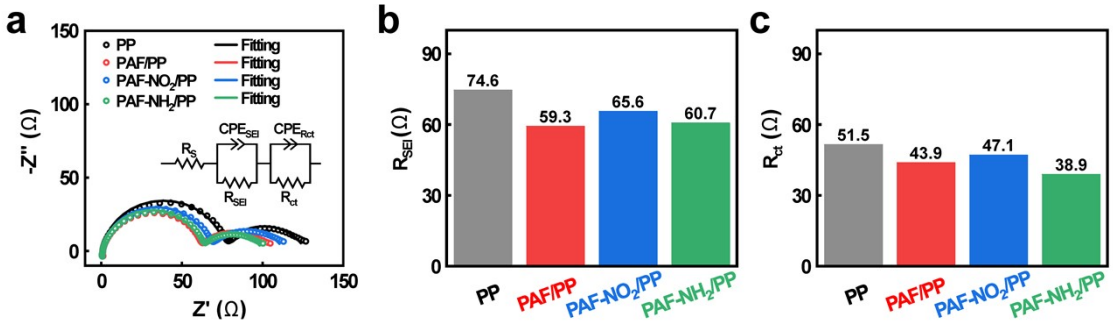

Fig. S9 (a) EIS spectra of Li|Li symmetric cells with PAF- and N-functionalized PAF-coated separators (inset: equivalent circuit model used for fitting, where R_s, R_{SEI}, and R_{ct} correspond to bulk electrolyte resistance, SEI resistance, and charge transfer resistance, respectively; CPE_{SEI} and CPE_{Rct} are constant phase elements that represent incomplete double-layer capacitance at the electrode surface). Comparison of (b) R_{SEI} and (c) R_{ct} values for PAF- and N-functionalized PAF-coated separators.

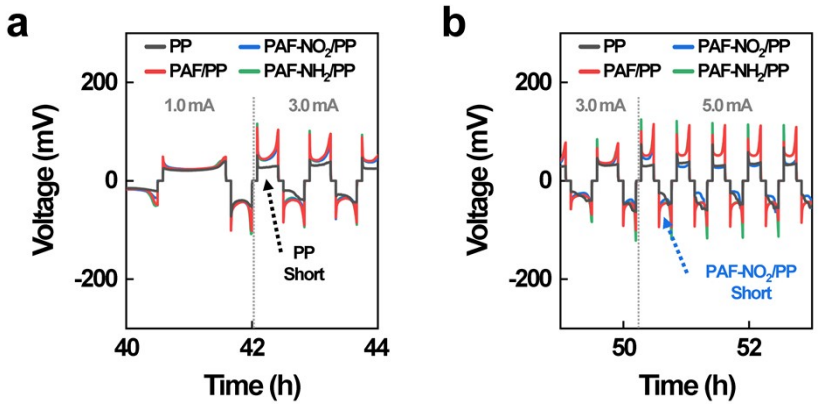

Fig. S10 Rate performance of Li|Li symmetric cells at current densities from 0.5 to 5.0 mA/cm^2 with a capacity of 1.0 mAh/cm^2, with a detailed representation of the short-circuiting points observed for cells using (a) the PP separator and (b) the PAF-NO_2/PP separator.

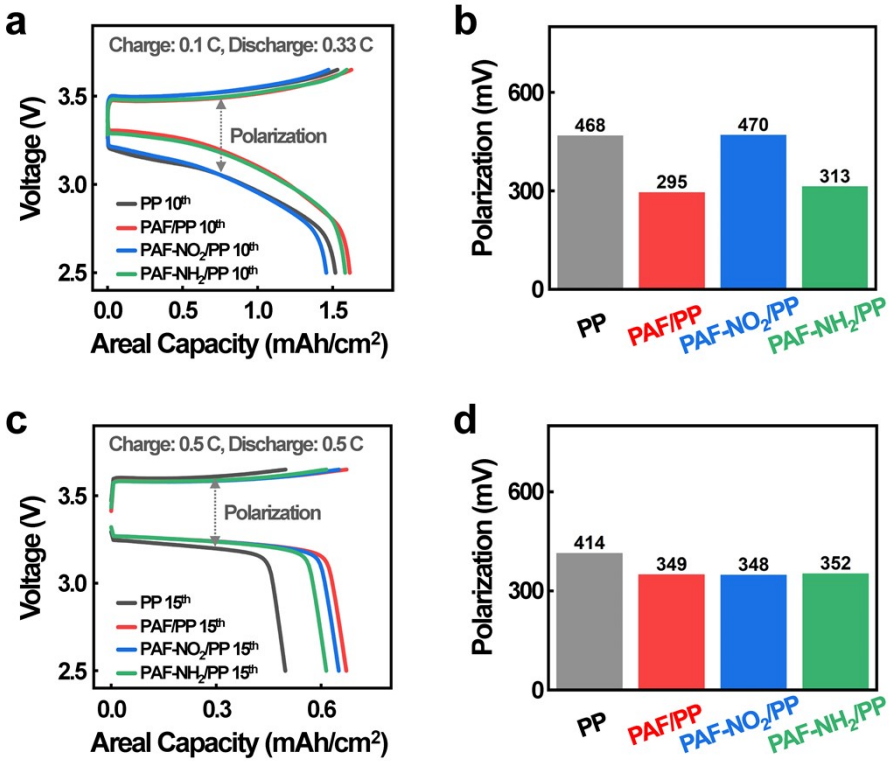

Fig. S11 (a) Charge/discharge curves of Li|LFP full cells at the 10th cycle, measured at a charge rate of 0.1 C and a discharge rate of 0.33 C within a voltage window of 2.5-3.65 V (vs. Li/Li^{+}), comparing PP and PAF-coated separators, along with (b) the corresponding polarization voltage at the mid areal capacity. (c) Charge/discharge curves of Li|LFP full cells at 0.5 C (within the rate performance range of 0.1-0.5 C) for PP and PAF-coated separators, and (d) the corresponding polarization voltage at the mid areal capacity.

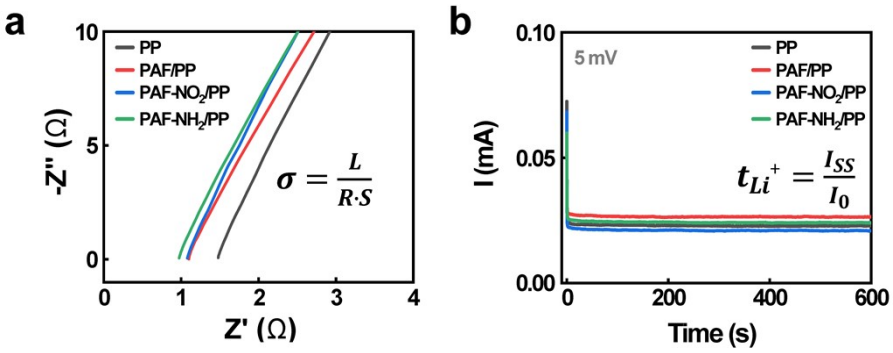

Fig. S12 (a) Nyquist impedance spectra of stainless steel/separator/stainless steel cells based on PAF- and N-functionalized PAF-coated separators (the equation for calculating ionic conductivity (σ) is presented, where L is the separator thickness, R is the bulk resistance, and S is the electrode area.). (b) Current-time curves of Li|separator|Li cells employing PAF- and N-functionalized PAF-coated separators (the equation for calculating the Li^+ transference number (t_{Li}^+) is shown, where I_0 and I_{SS} denote the initial and steady-state current values, respectively.).

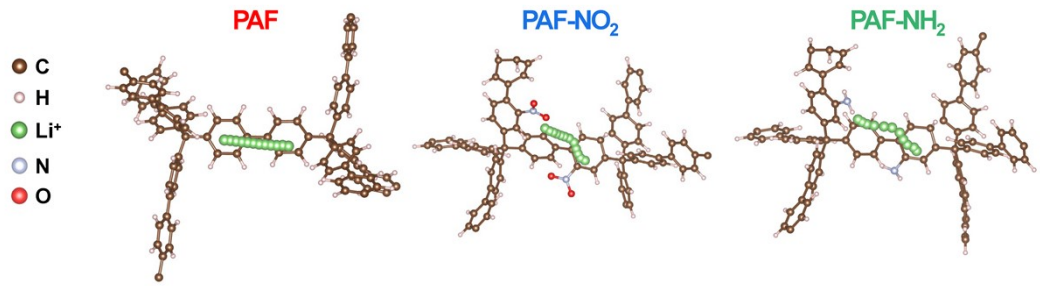

Fig. S13 Calculated Li^+ migration pathways between adjacent phenyl rings in pristine, NO_2-modified, and NH_2-modified PAFs.

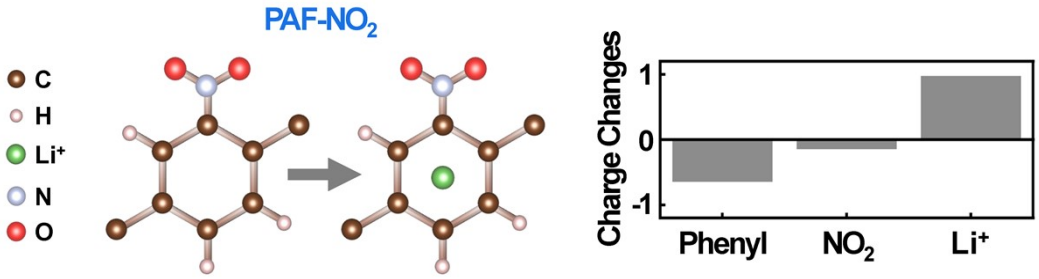

Fig. S14 Charge redistribution of the framework components in PAF-NO_2 and the adsorbed Li^+ when Li^+ is adsorbed onto the phenyl ring of PAF-NO_2.

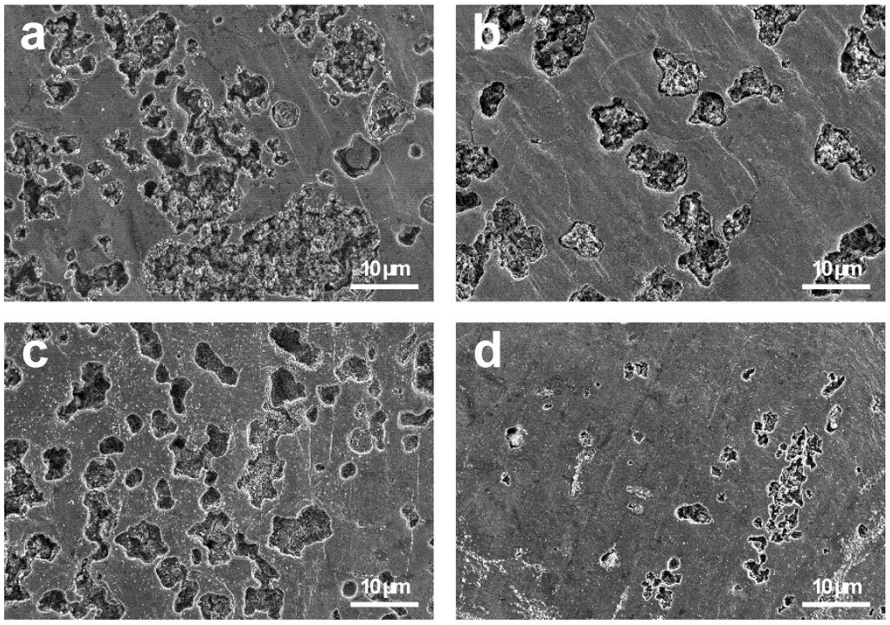

Fig. S15 FE-SEM images of the Li metal surface after one charge-discharge cycle in Li|LFP full cells using (a) PP, (b) PAF/PP, (c) PAF-NO_2/PP, and (d) PAF-NH_2/PP separators.

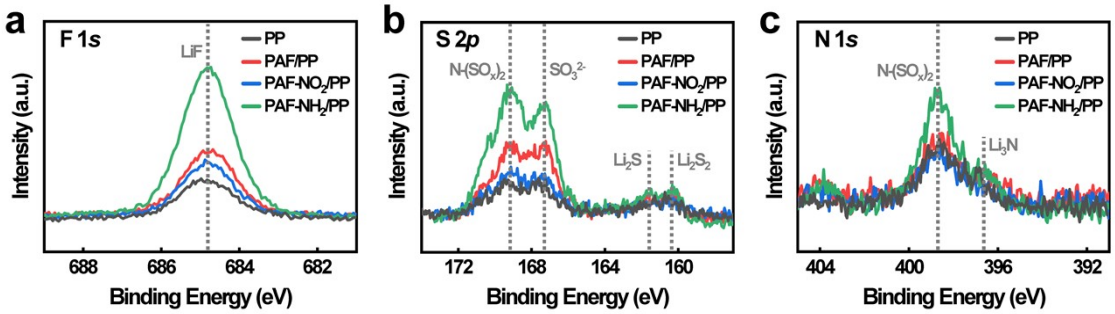

Fig. S16 XPS characterization of the SEI layers formed on the Li metal surface after one charge–discharge cycle in Li|LFP full cells with various separators. The spectra in the (a) F 1*s*, (b) S 2*p*, and (c) N 1*s* regions were obtained after Ar^+ (2 keV) etching for 40 s.

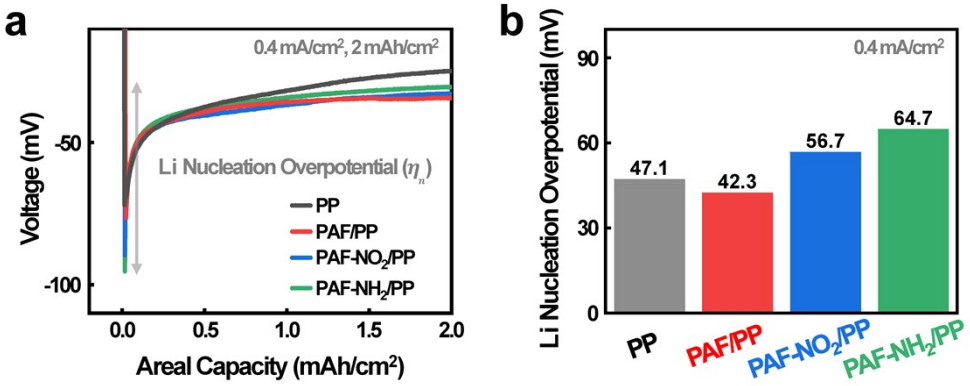

Fig. S17 (a) Voltage profile at the initiation of Li deposition at 0.4 mA/cm^2 with a capacity of 2.0 mAh/cm^2 for Li|Cu cells with different separators, and (b) Li nucleation overpotential during Li deposition in Li|Cu cells.

Table S1 Summary of XPS survey and elemental analysis results of PAF and N-functionalized PAFs, with the degree of N substitution expressed as the N/C atomic ratio (%).

	N-substituted degrees	XPS survey (at%)			
		C	O	N	N/C atomic ratio (%)
PAF	-	98.1	1.9	-	-
PAF-NO_2	1.0	89.9	6.5	3.6	4.0
PAF-NH_2	1.1	93.1	2.7	4.2	4.5

	N-substituted degrees	Elemental analysis (wt%)			
		C	H	N	N/C weight ratio (%)
PAF	-	94.9	5.1	-	-
PAF-NO_2	0.9	81.9	4.7	3.4	4.2
PAF-NH_2	0.8	87.5	4.6	3.1	3.6

Table S2 Summary of the porosity of the pristine PP separator and PAF- and N-functionalized PAF-coated separators. The porosity was determined based on the weight difference before and after *n*-butanol impregnation.[1, 2]

	W_d **(mg)**	W_w **(mg)**	V_d **(cm³)**	$Porosity$ (%)
PP	2.9	5.8	0.0071	51
PAF/PP	3.4	9.6	0.0099	77
PAF-NO_2/PP	3.4	8.6	0.0085	76
PAF-NH_2/PP	3.4	8.9	0.0085	80

The separator samples were first cut into circular pieces with a diameter of 1.9 cm and immersed in *n*-butanol for 2 h to ensure complete wetting. After immersion, excess *n*-butanol on the sample surface was gently removed using soft tissue, and the wet weight W_w was measured. The dry weight W_d and the volume V_d of the pristine separator were determined separately. The porosity was then determined using the equation below, where ρ_d represents the density of *n*-butanol. All values were averaged over three independent measurements.

$$Porosity\ (\%) = \frac{W_w - W_d}{\rho_d V_d}$$

Table S3 Summary of ion transport properties of the pristine PP separator as well as PAF- and N-functionalized PAF-coated separators. The Li^+ conductivity was calculated as the product of the overall ionic conductivity and the Li^+ transference number.

	Li^+ transference number	**Ionic Conductivity (mS/cm)**		
		Overall	**Anion**	**Cation (Li^+)**
PP	0.32	0.084	0.057	0.027
PAF/PP	0.45	0.158	0.087	0.071
PAF-NO_2/PP	0.31	0.138	0.096	0.042
PAF-NH_2/PP	0.40	0.153	0.092	0.061

Table S4 Summary of charge distributions upon Li^+ adsorption on pristine and N-substituted PAFs, including the framework components and the adsorbed Li^+.

	Li^+	PAFs			
		Overall	**Phenyl**	**NO_2**	**NH_2**
PAF	-	0.03	0.03	-	-
PAF–Li^+	0.98	-0.55	-0.55	-	-
PAF-NO_2	-	0.11	0.61	-0.50	
PAF-NO_2–Li^+	0.74	-0.35	0.47	-0.82	
PAF-NH_2	-	0.10	0.53	-	-0.43
PAF-NH_2–Li^+	1.02	-0.75	-0.29	-	-0.46

Table S5 XPS chemical compositions of the Li metal surface obtained after one charge-discharge cycle in Li|LFP full cells with various separators. Atomic percentages were determined after Ar^+ (2 keV) etching for 0, 40, 80, and 120 s.

Separator	Etching time (s)	Chemical composition (Atomic %)						F/C	(F+S+N)/C
		C	F	Li	N	O	S		
PP	0	29.41	1.31	33.73	1.86	32.55	1.14	**0.04**	**0.15**
	40	14.12	1.50	41.62	0.84	41.14	0.78	**0.11**	**0.22**
	80	12.23	1.30	43.70	0.60	41.61	0.56	**0.11**	**0.20**
	120	10.65	0.95	46.09	0.62	41.26	0.43	**0.09**	**0.19**
PAF/PP	0	14.23	1.02	49.58	0.95	33.28	0.94	**0.07**	**0.20**
	40	14.29	2.01	42.61	0.88	38.86	1.36	**0.14**	**0.30**
	80	15.31	2.01	40.40	0.67	40.72	0.89	**0.13**	**0.23**
	120	15.34	1.58	40.43	0.57	41.48	0.59	**0.10**	**0.18**
PAF-NO_2/PP	0	26.72	1.1	37.39	1.27	32.4	1.12	**0.04**	**0.13**
	40	15.15	1.54	39.13	0.64	42.8	0.73	**0.10**	**0.19**
	80	14.25	1.21	40.38	0.47	43.16	0.53	**0.08**	**0.16**
	120	11.97	0.84	44.7	0.43	41.64	0.42	**0.07**	**0.14**
PAF-NH_2/PP	0	18.91	2.67	41.28	1.77	32.9	2.47	**0.14**	**0.37**
	40	13.96	4.49	38.62	1.26	39.3	2.37	**0.32**	**0.58**
	80	13.35	3.69	39.77	0.94	40.65	1.6	**0.28**	**0.47**
	120	11.97	2.85	43.02	0.79	39.89	1.49	**0.24**	**0.43**

References

1. J. Zhu, M. Yanilmaz, K. Fu, C. Chen, Y. Lu, Y. Ge, D. Kim and X. Zhang, *J. Membr. Sci.*, 2016, **504**, 89-96.
2. C. Likitaporn, M. Okhawilai, P. Kasemsiri, J. Qin, P. Potiyaraj and H. Uyama, *Sci. Rep.*, 2022, **12**, 19915.